Excess protons in water-acetone mixtures

Rocío Semino, and Daniel Laria

Citation: The Journal of Chemical Physics **136**, 194503 (2012); doi: 10.1063/1.4717712
View online: https://doi.org/10.1063/1.4717712
View Table of Contents: http://aip.scitation.org/toc/jcp/136/19
Published by the American Institute of Physics

Excess protons in water-acetone mixtures

Rocío Semino[1] and Daniel Laria[1,2,a)]
[1]*Departamento de Química Inorgánica Analítica y Química e INQUIMAE, Facultad de Ciencias Exactas y Naturales, Pabellón II, Ciudad Universitaria, (1428) Capital Federal, Argentina*
[2]*Departamento de Física de la Materia Condensada, Comisión Nacional de Energía Atómica, Av. Gral. Paz 1499 (1650) San Martín, Prov. de Buenos Aires, Argentina*

(Received 13 March 2012; accepted 27 April 2012; published online 17 May 2012)

Using molecular dynamics experiments, we analyze equilibrium and dynamical characteristics related to the solvation of excess protons in water-acetone mixtures. Our approach is based on the implementation of an extended valence-bond Hamiltonian, which incorporates translocation of the excess charge between neighboring water molecules. Different mixtures have been analyzed, starting from the pure water case down to solutions with a water molar fraction $x_w = 0.25$. In all cases, we have verified that the structure of the first solvation shell of the H_3O^+ moiety remains practically unchanged, compared to the one observed in pure water. This shell is composed by three water molecules acting as hydrogen bond acceptors, with no evidence of hydrogen bond donor-like connectivity. Moreover, the increment in the acetone concentration leads to a gradual stabilization of Eigen-like $[H_3O \cdot (H_2O)_3]^+$ configurations, in detriment of Zundel-like $[H \cdot (H_2O)_2]^+$ ones. Rates of proton transfer and proton diffusion coefficients have been recorded at various water-acetone relative concentrations. In both cases, we have found a transition region, in the vicinity of $x_w \sim 0.8$, where the concentration dependences of the two magnitudes change at a quantitative level. A crude estimate shows that, at this tagged concentration, the volumes "occupied" by the two solvents become comparable. The origins of this transition separating water-rich from acetone-rich realms is rationalized in terms of modifications operated in the nearby, second solvation shell, which in the latter solutions, normally includes at least, one acetone molecule. Our results would suggest that one possible mechanism controlling the proton transfer in acetone-rich solutions is the exchange of one of these tagged acetone molecules, by nearby water ones. This exchange would give rise to Zundel-like structures, exhibiting a symmetric, first solvation shell composed exclusively by water molecules, and would facilitate the transfer between neighboring water molecules along the resonant complex.
 [http://dx.doi.org/10.1063/1.4717712]

I. INTRODUCTION

Aqueous protons represent singular electrolytes in solution chemistry. Despite their apparent simplicity, it was not until very recently that the solvation structure of these cations has been unraveled. Historically, two moieties had been proposed as possible stable structures describing the solvation of excess protons: the tricoordinated Eigen[1] cation $[H_3O \cdot (H_2O)_3]^+$ and the resonant Zundel[2] dimer $[H \cdot (H_2O)_2]^+$. In this respect, results from computer simulations, obtained with different degrees of quantum detail, have been particularly enlightening and agree in providing a unified description of the microscopic arrangement of water molecules around the excess charge.[3–15] The present picture that emerges from this body of simulation experiments portrays aqueous protons as "fluxional defects," embedded within a tridimensional network of hydrogen-bonded water molecules. In fact, these defects include a series of intermediate structures – including the Zundel and Eigen cations as limiting configurations with clear geometrical arrangements – which interconvert between each other, along characteristic ∼1 ps time intervals. Not surprisingly, these timescales coincide with the ones modulating the process of breaking and subsequent reconstruction of hydrogen bonds (HBs) in pure water.[16,17] The changes in the architecture of hydrogen bonds not only do they promote modifications of the proton solvation structures but have important consequences on the dynamical description of the excess charge as well. Most notable, are the mechanisms that control proton transfers between neighboring water molecules which, in turn, give rise to the unusually high mobility of protons in aqueous media operated via the classical Grotthuss translocation mechanism.[18]

The addition of aprotic co-solvents to neat aqueous phases introduces important disruptions in the original HB connectivity pattern. To a large extent, these modifications are the consequence of the exclusive HB-acceptor characteristics of those species, which contrast with the dual HB donor-acceptor character of water. Liquid phases combining, water on the one hand, and acetonitrile, dimethylsulfoxyde or acetone, on the other one, represent prototypical binary solutions that fully mix at all compositions, at ambient conditions. Consequently, they provide ideal testing grounds for monitoring the gradual changes that take place in the water original tridimensional HB network as one increases the concentrations of aprotic components. Within this context, it is interesting

a)E-mail: dhlaria@cnea.gov.ar.

to investigate how these modifications, in turn, are reflected in the resulting solvation structure and dynamics of solvated protons.

Gileadi *et al.*[19,20] have analyzed proton transport in aqueous mixtures involving acetonitrile as aprotic co-solvent. They conclude that, in solutions with water contents above $\sim 10 - 20$ vol. % (which is roughly equivalent to molar fractions $x_w \gtrsim 0.25$), the hopping Grotthuss-like mechanism contributes to the charge transport in a sensible fashion. Contrasting, the addition of 20 vol. % of acetonitrile to pure water phases does not promote meaningful modifications in the proton conductivity. Moreover, Gileadi *et al.* provide a physical interpretation of their results based on considerations involving local concentration fluctuations in the vicinity of the excess charge, leading to aqueous "clustered" domains.

In the present paper, we present a complementary approach to the analysis of these solutions based on results from molecular dynamics simulation experiments. In particular, we have analyzed equilibrium and dynamical characteristics of excess protons dissolved in water-acetone solutions, covering a wide range of individual solvent concentrations. Our study is akin to two previous analyses, in which the behavior of protons in water/methanol solutions have been examined.[21,22] However, the characteristics of the intramolecular connectivity between the two polar components examined here differ from the one presented in previous studies at a qualitative level. In the former cases, both solvents present dual HB donor/acceptor characteristics; this feature, in turn, might open the possibility of protons transfers operated by the Grotthuss-like mechanism, similar to the one prevailing in pure water, through the following "MeOH bridged" sequence:

$$H_3O^+ + MeOH + H_2O \rightarrow H_2O + MeOH_2^+$$
$$+ H_2O \rightarrow H_2O + MeOH + H_3O^+.$$

Although the real importance of this proton transfer channel is still under debate,[21,22] it is certainly absent in protic/aprotic mixtures, where the topology of HBs restricts proton shuttles to spatial domains involving exclusively water molecules.

To undertake our simulation experiments we implemented a multi-state empirical valence bond (MS-EVB) model Hamiltonian. This approach has been pioneered by Warshel and collaborators,[23–25] and has been successfully implemented to analyze a variety of aqueous environments,[26] such as condensed phases,[3–5,10–13] water/air interfaces,[27,28] porous media,[29] nanochannels,[30,31] strong-acid solutions,[32] reverse micelles,[33] and supercritical states,[34] to cite a few relevant examples. As such, the implementation of the MS-EVB model for the case of protons dissolved in protic/aprotic mixtures, in which the aprotic component has a low proton affinity, is fairly straightforward. In what follows, we will show evidence that would suggest that the changes operated in the proton transfer and diffusion mechanisms are the consequences of the modifications operated in the connectivity pattern and the dynamics of HBs at the close vicinity of the excess protons, and do not seem to be dependent on long-wavelength concentration fluctuations involving mesoscopic spatial domains.

The organization of the present paper is as follows: in Sec. II, we will present a brief detail of the simulation procedure and the parametrization of the MS-EVB Hamiltonian. The main results of our research appear in Sec. III whereas the concluding remarks are summarized in Sec. IV.

II. MODEL

The systems under investigation were composed of a single proton dissolved in different W-A solutions. Seven concentrations, characterized by water molar fractions $x_w = 1$, 0.9, 0.8, 0.7, 0.6, 0.5, and 0.25, were examined. The simulated systems were fully periodic and were confined within cubic boxes, whose lengths were adjusted so as to bring the global densities of the mixtures in agreement with experimental information at ambient conditions.[35] In passing from $x_w = 1$ down to $x_w = 0.25$, the magnitudes of the box lengths were intermediate between 15 Å and 22 Å. The time step was set to $\Delta t = 0.5$ fs. All simulation experiments were preceded by initial equilibration runs of $\sim$100 ps, during which atomic velocities were repeatedly rescaled, to provide stable runs at T close to 298 K. At each concentration, statistics were collected along three independent, microcanonical trajectories, each one lasting typically $\sim$2 ns. Long range interactions originated from different Coulomb contributions were handled using Ewald sum techniques, assuming the presence of a uniform neutralizing background.

The trajectories were generated using an MS-EVB approach. The implementation of this methodology has been extensively described in a series of previous studies, so we will briefly describe here its main features and refer the interested reader to Refs. 10–13 for additional details. Basically, the dynamics of the nuclei with coordinates $\{\mathbf{R}\}$ was driven by forces derived from $\epsilon_0(\{\mathbf{R}\})$, the ground state potential energy surface of an EVB Hamiltonian of the type,[23–25]

$$\hat{H}_{EVB}(\{\mathbf{R}\}) = \sum_{ij} |\phi_i\rangle h_{ij}(\{\mathbf{R}\})\langle\phi_j| \,. \tag{1}$$

In the previous equation, the kets $\{|\phi_i\rangle\}$ represent the elements of a diabatic basis set, each one describing configurations in which the excess proton is localized in a particular water molecule. The low proton affinity of the A molecules, led us to disregard the inclusion of diabatic states localized in carbonyl groups. In fact, experimental information shows that, in aqueous media, protonated acetone $[(CH_3)_2CO \cdot H]^+$ (pKa ~ -7.2) (Ref. 36) behaves as a much stronger acid than the hydronium $[H_3O]^+$ group (pKa ~ -1.7). Note that this description may not be totally appropriate in solutions with very low W-concentrations, i.e., $x_w \lesssim 0.2$, where a more correct description of the proton-A interactions and the eventual incorporation of A-centered diabatic states should be critically evaluated. Consequently, this concentration regime was not explored in the present study.

The ground state $|\psi_0\rangle$ of the $\hat{H}_{EVB}$ satisfies

$$\hat{H}_{EVB}|\psi_0\rangle = \epsilon_0(\{\mathbf{R}\})|\psi_0\rangle \tag{2}$$

and can be expressed in terms of the diabatic basis as

$$|\psi_0\rangle = \sum_i c_i |\phi_i\rangle. \tag{3}$$

Invoking the Hellman-Feynman theorem,[37] the dynamics of the kth classical nucleus of mass M_k is governed by the following Newton equation:

$$M_k \frac{\mathrm{d}^2\mathbf{R}_k}{\mathrm{d}t^2} = -\langle\psi_0|\nabla_{\mathbf{R}_k}\hat{\mathrm{H}}_{\mathrm{EVB}}|\psi_0\rangle = -\sum_{ij} c_i c_j \nabla_{\mathbf{R}_k} h_{ij}(\{\mathbf{R}\}). \tag{4}$$

At each step of the simulation, the different water molecules participating in the diabatic-state basis set were determined by establishing a connected network of hydrogen bonded molecules, started at the position of the excess charge (hereafter referred to as a pivot water and denoted $[H_3O^*]^+$). The tagged molecule was updated along the simulation run so as to coincide with the instantaneous diabatic state exhibiting the largest c_i^2. Typically, the number of diabatic states involved in the construction of the MS-EVB Hamiltonian varied from ∼15 for pure water, down to ∼7 for $x_w = 0.25$.

A key element in the MS-EVB approach is the proper parametrization of the different matrix elements $h_{ij}(\{\mathbf{R}\})$. Normally, such procedure involves bringing the MS-EVB results for the geometry and energetics of $[H\cdot(H_2O)_n]^+$ clusters, in reasonable agreement with those obtained from highly optimized quantum calculations. For the case of aqueous protons, several EVB Hamiltonian models are available;[10–13] although the most recent developments clearly yield improvements in the descriptions at a quantitative level, the qualitative features and trends obtained from practically all of them, are physically sound. Yet, the incorporation of acetone as a co-solvent imposes a series of previous considerations, even in the absence of the excess charge. In particular, previous simulation experiments have shown that the direct implementation of transferable potentials is not always recommended, since it may lead to unphysical results, related to demixing and phase separation phenomena.[38] The general conclusion that emerges from these simulations suggests that several of the usual combinations of force fields, originally tailored to model pure liquid phases, fail to provide a reasonable description of the structures of W-A mixtures. One exception to these cases is, perhaps, the combinations involving the acetone model developed by Weerasinghe and Smith (WS) (Ref. 39) and the classical SPC/E water model.[40] Yet, some aspects related to the suitability of this particular choice remain debatable and await additional clarifications.[41–43] Consequently, our first concern was to look for a combination of A and W Hamiltonian models that (i) would yield homogeneous mixtures along the whole concentration range and (ii) could also be implemented within an EVB-Hamiltonian scheme. After several attempts, we found that the flexible TIP3P (Ref. 44) -WS combination, implemented via the usual means for cross interactions, yields structural results that do not show signs of phase separation for sufficiently large systems – say, with a total number of molecules close to ∼2000 – along time spans of several tens of nanoseconds. Moreover, the subsequent incorporation of this combination of site-site pair potentials within the MS-EVB1 scheme proposed by Schmitt and Voth,[10] yielded stable trajectories after relaxing the criterion of the algorithm for choosing the diabatic states participating in the instantaneous EVB Hamiltonian.[10] In particular, we stretched the original H···O threshold connectivity distance from $r_{\mathrm{thr}} = 2.3$ Å up to $r_{\mathrm{thr}} = 3.0$ Å. In doing so, we prevented sizeable energy discontinuities, originated in sporadic concentration fluctuations which, otherwise, would bring the number of water molecules in the pivot first solvation shell down to two, reducing the total number of diabatic states by a factor of ∼3. This simple modification allowed to control the energy conservation below 2%−3%, along trajectories lasting typically 2–3 ns. We finally remark that, in W-A solutions, we have not encountered a significant number of configurations, in which the pattern of HBs would include bifurcations such as those described in Fig. 1 of Ref. 12.

III. RESULTS

A. Solvation structures

We start our analysis by focusing attention on the structural characteristics of the solvation of the excess proton in different W-A mixtures. This information can be readily obtained from site-site spatial correlations of the type,

$$\rho_{\mathrm{o}^*\alpha}(r) = \frac{1}{4\pi r^2}\left\langle \sum_i \delta\left(\left|\mathbf{r}_i^{\alpha} - \mathbf{r}_{\mathrm{o}^*}\right| - r\right)\right\rangle; \tag{5}$$

where $\mathbf{r}_{\mathrm{o}^*}$ denotes the coordinate of the instantaneous pivot site and $\mathbf{r}_i^{\alpha}$ is the coordinate of the ith site of species α. In Eq. (5), $\langle\cdots\rangle$ represents an equilibrium ensemble average. Results for $\rho_{\mathrm{o}^*\alpha}(r)$ for a few relevant solvent sites are displayed in the top and middle panels of Fig. 1. The top one includes correlations involving oxygen sites in W molecules: in all cases, the curves are dominated by prominent peaks located at $r \sim 2.55$ Å, involving three, tightly bound water molecules. At all concentrations, these molecules comprise the first solvation shell of the excess charge and act as HB acceptors from the central pivot hydronium. Additional peaks, very much attenuated, at $r \sim 4.5$ Å are also clearly perceptible and correspond to W molecules located in the second solvation shell. Spatial correlations involving pivot-H atoms in water molecules (not shown) reveal the absence of H–O–H ... $[O^*H_3]^+$ connectivity. It has been demonstrated[10,11] that the localization of the excess positive charge in the pivot prevents such connectivity pattern.

The coordination of the pivot with oxygen sites in carbonyl groups of A is shown in the middle panel. The first peaks at $r \sim 3$ Å correspond to rare H_2O^*H ... $OC(CH_3)_2$ connectivity (in passing, note the differences in practically one order of magnitude between these peaks and the ones in the top panel), whereas the most relevant structures appear at $r \sim 4.5$ Å. These broader peaks correspond to A molecules lying in the proton second solvation shell that act as HB acceptors from inner W molecules located in the first solvation shell. As expected, the number of A molecules in the second solvation shell increases as we move towards A richer solutions; for example, at the lowest water molar fraction investigated, $x_w = 0.25$, one normally observes, ∼3 acetone molecules lying in this region. Finally, and in agreement with

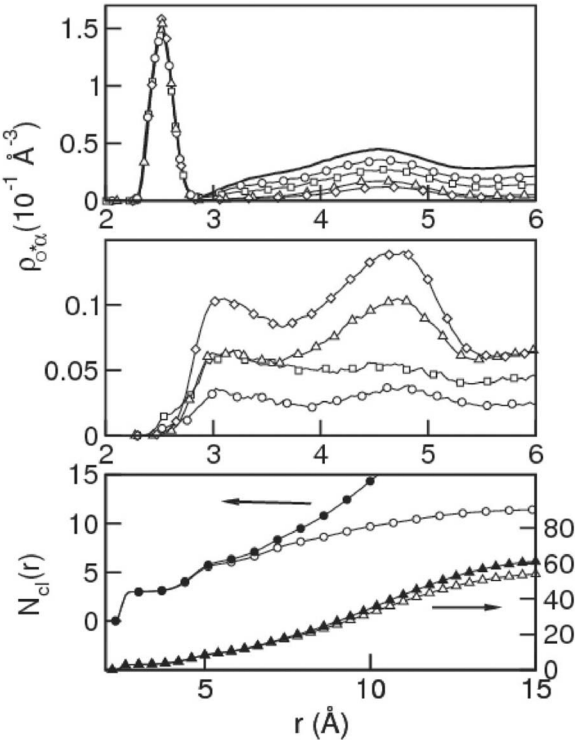

FIG. 1. Pivot-oxygen water (top panel) and pivot-oxygen acetone (middle panel) site-site pair correlation functions for W-A solutions with concentrations $x_w = 1$ (solid line), $x_w = 0.9$ (circles), $x_w = 0.8$ (squares), $x_w = 0.5$ (triangles), and $x_w = 0.25$ (diamonds). Bottom panel: Cumulative integrals of the pivot-oxygen water connectedness correlation function (open symbols) for representative $\mathcal{A}$-type mixtures with $x_w = 0.5$ (triangles, right y-axis) and $x_w = 0.25$ (circles, left y-axis). Also shown are results for cumulative integrals of the corresponding pair correlation function (black symbols).

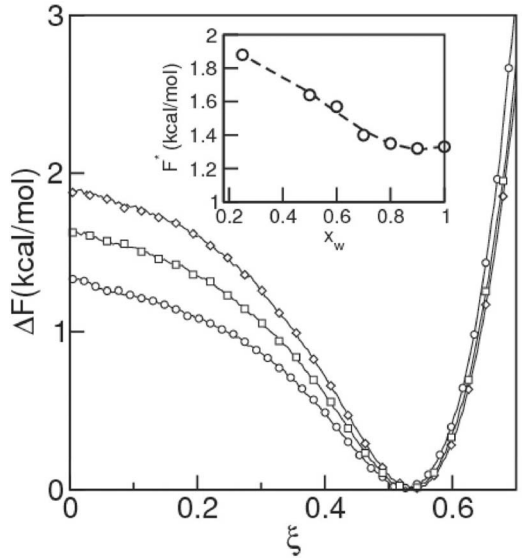

FIG. 2. Free energy associated with the Zundel-Eigen order parameter ξ (see text) for different W-A solutions: $x_w = 1$ (circles); $x_w = 0.5$ (squares); $x_w = 0.25$ (diamonds). In the inset we present the concentration dependence of the free energy barrier for Zundel-Eigen interconversions.

previous results obtained in MeOH-H_2O mixtures,[21,22] the analysis (not shown) of the solvation structure of the closest shell at the vicinity of the "hydrophobic" cap region of the H_3O^+ moiety, comprises exclusively distal CH_3 groups in A.

As it was mentioned in Sec. I, in aqueous media, proton states are normally portrayed in terms of "fluxional defects," involving a series of intermediate moieties between two well defined solvation structures: the centro-symmetric $[H_3O \cdot (H_2O)_3]^+$ Eigen cation and the resonant $[H \cdot (H_2O)_2]^+$ Zundel dimer. Within this context, one important aspect to be explored concerns the relative stability of these limiting configurations. Voth *et al.*[10,11] have addressed this issue resorting to free energies associated with a a simple order parameter ξ, namely,

$$F(\xi_0) \propto -\ln\langle\delta(\xi - \xi_0)\rangle, \tag{6}$$

where ξ is related to the magnitude of the coefficients c_i, namely,

$$\xi = c_1^2 - c_2^2, \tag{7}$$

where c_1 and c_2 represent the two largest coefficients in the expansion shown in Eq. (3). Profiles for $F(\xi)$ at high, intermediate and low water concentrations are shown in Fig. 2. In all cases, one observes that Eigen cations remain the most stable configurations and are characterized by $\xi \sim 0.54$. Moreover, resonant Zundel structures, characterized by values of $\xi \sim 0$ become gradually more infrequent, as the water content in the solutions diminishes, a fact that could reveal some weakening in the HB structure that controls the delocalization of the proton along the bond joining Zundel-partners and, eventually, a reduction in the magnitude of the instantaneous polarization fluctuations, in solutions with lower water contents. To gain quantitative discern about this trend, in the inset of Fig. 2 we present the concentration dependence of the magnitude of the free energy barrier, namely, $F^* = \Delta F(\xi = 0)$, for Eigen-Zundel interconversions. Interestingly, for x_w down to ~0.8, the value of F^* remains practically constant at ~1.35 kcal mol^{-1} whereas as we move to lower water content solutions, the magnitude of the barrier presents a steady increment, reaching ~1.9 kcal mol^{-1} at $x_w = 0.25$. As such, these results would suggest the onset of changes at a qualitative level in the prevailing solvation structure of the proton in the concentration range $x_w \sim 0.8$. As we will see shortly, these modifications manifest in a similar fashion in the concentration dependence of dynamical properties of the excess proton. Consequently, and for clarity purposes, we prefer to postpone any further discussions about this issue for Sec. III B.

B. Proton transfer

To get a first notion of the modifications operated in the rate of proton transfer in aqueous solutions with the increment of an aprotic co-solvent, it will be useful to examine the results depicted in Fig. 3. Panels (a), (b), and (c) contain time evolutions of the pivot-oxygen label along fairly long, 100 ps trajectories for mixtures with $x_w = 1$, 0.8 and 0.25, respectively. In the three cases, the plots comprise sequences of horizontal lines interrupted by episodes, during which the pivot label resonates between two neighboring water molecules, following the stabilization of a "special partner" structure, i.e., a distorted Eigen-like cation with a preferential coordination

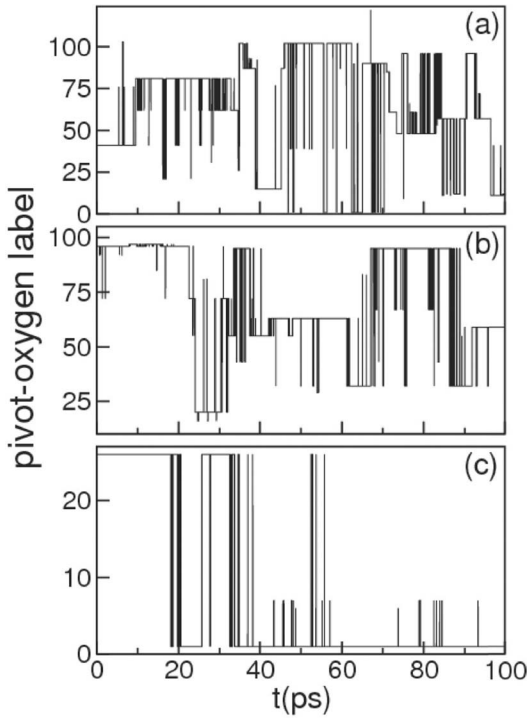

FIG. 3. Time dependence of pivot-oxygen label in different W-A mixtures. (a): $x_w = 1$; (b): $x_w = 0.8$; (c): $x_w = 0.25$.

between the central molecule and a tagged one located in the first solvation shell.[45,46] In addition, one also observes a few occasional spikes, which correspond to aborted transfer attempts. At a first glance, in the upper panel, one can identify ∼20 different oxygen-pivots, whereas in $x_w = 0.8$ solutions, that number drops practically by a factor of ∼2. These modifications are even more dramatic in panel (c), where along a 100 ps time span, the number of transfers and resonance episodes fall down to ∼4, involving the same two partners, i.e., oxygen atoms with labels 1 and 26.

The previous description can be cast in more quantitative terms by resorting to the analysis of time correlation functions. Following previous studies,[11] we focussed attention on temporal correlations of the type,

$$C(t) = \frac{\langle \delta h_i(t) \cdot \delta h_i(0) \rangle}{\langle (\delta h_i)^2 \rangle}, \tag{8}$$

where the characteristic function $h_i(t)$ is equal to 1 if the pivot label at time t corresponds to the ith water molecule and 0 otherwise. In Eq. (8) $\delta\mathcal{O}(t) = \mathcal{O}(t) - \langle\mathcal{O}\rangle$ represents the instantaneous fluctuation of the observable $\mathcal{O}$ at time t, away from its equilibrium value.

Assuming a first-order kinetics behavior, linear response theories predict that the corresponding proton transfer rates k_{PT} can be obtained from the limiting slopes, namely,

$$k_{PT} = \lim_{t\to\infty} -\frac{\mathrm{d}\ln C(t)}{\mathrm{d}t}. \tag{9}$$

In Fig. 4, we present results for $\ln C(t)$. In all cases, the curves present an initial sub-picosecond decay associated with "rattle" episodes,[47] i.e., pivot interchanges along preferential bonds,[45,46,48] that can be analyzed in terms of more refined population relaxation analyses.[49] After approximately

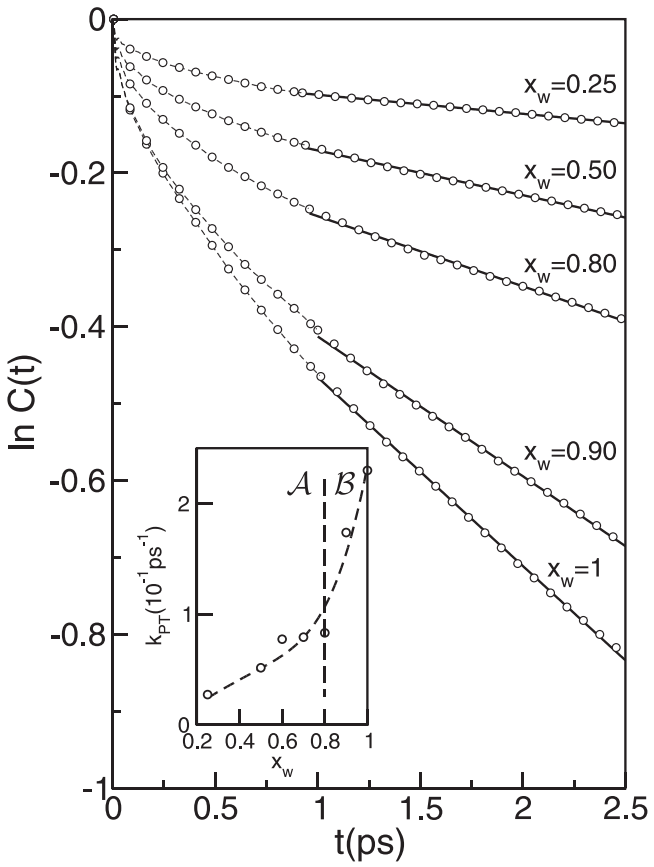

FIG. 4. Population relaxations of the pivot-oxygen label for different W-A solutions (circles). The solid lines represent linear fits for $t \gtrsim 1$ ps intervals. The inset shows results for rates of proton transfer as a function of the water molar fraction obtained from the fits.

a 1 ps time interval, all curves look reasonably linear. The inset of the figure includes results for the rates as a function of the composition of the solvent mixture, extracted from linear fits of $\ln C(t)$ for $t \gtrsim 1$ ps. In passing from pure water down to an $x_w = 0.25$ solution, the characteristic timescale describing proton jumps stretches by approximately one order of magnitude. More interestingly, the dependence of k_{PT} with x_w looks non-uniform; note that the dashed-curve that helps the eye presents a "kink" in the $x_w \sim 0.8$ region. A crude estimate based on the differences in the densities of the two solvents at ambient conditions, $\rho_w/\rho_A \sim 4$, shows that the $x_w \sim 0.8$ concentration regime corresponds to liquid phases in which both solvents "occupy" similar volumes. To facilitate our description, in what follows, we will denote A-rich solutions, i.e., $x_w \lesssim 0.8$ as of type $\mathcal{A}$ and W-rich solutions, i.e., $x_w \gtrsim 0.8$ as of type $\mathcal{B}$ (see Fig. 4).

The origins of the drastic drop and the changes in the functionality of k_{PT} with the increment of A, can be traced back to the modifications in the solvation structure prevailing at the close vicinity of the excess charge. These modifications, in turn, should also correlate with changes in the microscopic mechanisms that control the transfer processes. Even for the simpler case of adiabatic proton transfer processes in pure water, the description of such mechanisms is not straightforward, since they are the result of a complex interplay between polarization fluctuations of the environment and the dynamics of

the three dimensional HB network in the vicinity of the excess charge. At present there seems to be sufficient consensus supporting the idea that a key element governing proton transfer in water is a HB cleavage taking place in the second solvation shell.[6,7,45,46,48–50]

The addition of aprotic co-solvents to water brings new elements that require a more detailed analysis; in particular, those related to local concentration fluctuations in the close vicinity of the proton. Still, it seems reasonable to anticipate that the proton transfer mechanisms found in pure water should also prevail in $\mathcal{B}$-type solutions, so we will not analyze this regime in much detail. For the other limiting case, i.e., $\mathcal{A}$-type solutions, we made a comprehensive analysis of different geometrical parameters along tens of transfer episodes, at different compositions. The main conclusions of our observations can be inferred from the results shown in the plots of Fig. 5 and the schemes of Fig. 6. The panels of Fig. 5 include time evolutions of a few selected parameters, taken along one particular transfer episode, in an $x_w = 0.25$ solution. In the top one, we display results for the pivot-oxygen label. To facilitate our description, we have set the temporal origin at the onset of the proton stabilization in the new pivot, as it gets transferred from the donor W_1 to the acceptor W_2 water molecules (labelled 29 and 17, respectively). Panel (b) includes results for the asymmetric stretch coordinate, namely,

$$\xi(t) = \left|\mathbf{r}^{o}_{29}(t) - \mathbf{r}_P(t)\right| - \left|\mathbf{r}^{o}_{17}(t) - \mathbf{r}_P(t)\right|, \qquad (10)$$

where $\mathbf{r}_P$ corresponds to the coordinate of the resonant proton. Clearly, the spikes episodes and resonance intervals correlate

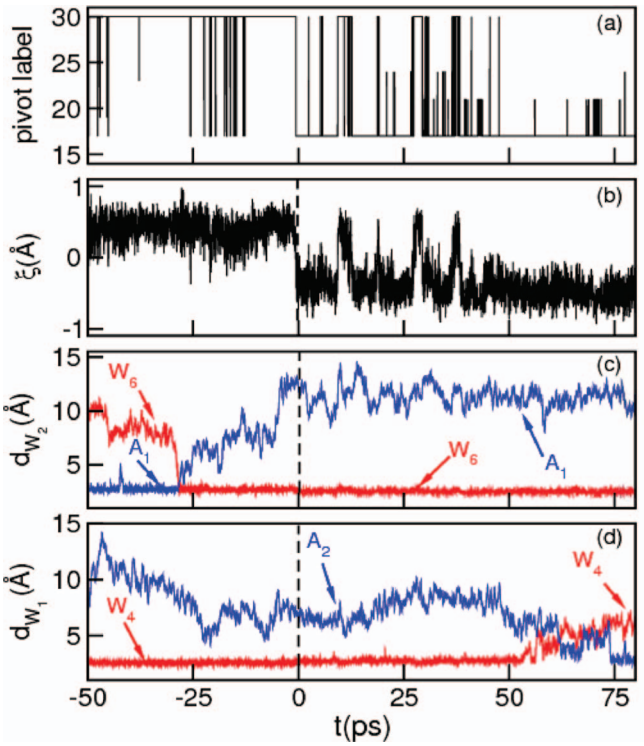

FIG. 5. Time evolution of the different parameters along a proton transfer episode in an $x_w = 0.25$ W-A solution. (a): Pivot label; (b): Asymmetric stretch coordinate (see text); (c): Distance between the center of mass of water molecule W_2 and nearby water and acetone molecules W_6 and A_1 (see Fig. 6); (d): Same as (c), for water molecule W_1 and nearby water and acetone molecules W_4 and A_2 (see Fig. 6).

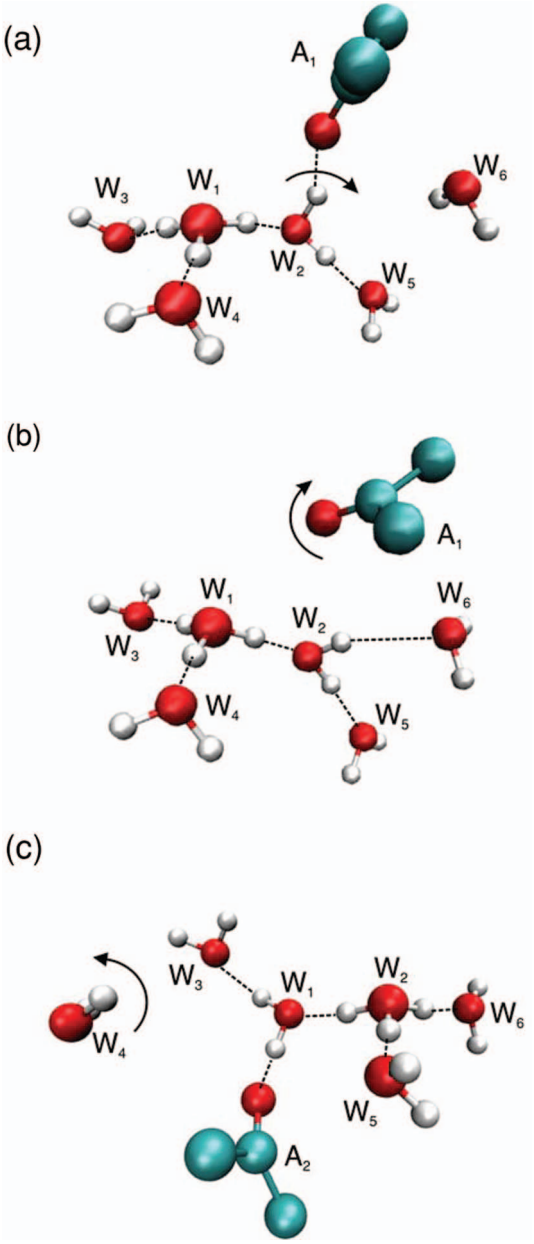

FIG. 6. Snapshots of selected configurations along the proton transfer episode described in Fig. 5. (a) $t = -50$ ps; (b) $t = -30$ ps; (c) $t = 70$ ps.

with events during which $\xi(t)$ changes sign, very likely following polarization fluctuations of the local environment.

To move forward, we then analyzed the solvation structure at negative times. As expected, for $t \sim -50$ ps, the first solvation shell of the W_1 pivot is composed exclusively by three water molecules, W_2, W_3, and W_4, whereas the second solvation shell contains three acetone molecules and three water molecules, all acting as HB acceptors from water molecules comprising the Eigen moiety (see Fig. 6(a)). For the purposes of the present discussion, we will focus our attention on W_2 – the next pivot – which originally acts as double HB donor to molecules W_5 and A_1. Note that, should this intermolecular connectivity pattern had remained without modifications, after an eventual proton transfer, the coordination of the new $[H_3O^*]^+$ pivot, localized at W_2, would have

included the acetone molecule A_1 as part of its first solvation shell, giving rise to a highly unfavorable hydronium solvation structure.

Panels (c) and (d) in Fig. 5 display the time evolutions of the distance d_{W_i} between the centers of mass of the "special partners"[45,46] ($i = 1, 2$) and a few relevant nearby molecules. In the case of panel (c) we have recorded the distances between W_2 and acetone A_1 (blue line in Fig. 5(c)) and also the distance to an originally uncoordinated, W_6 molecule (red line in Fig. 5(c)). Note that a key process, giving rise to a much favorable transfer process, takes place at $t \sim -30$ ps: molecule A_1 detaches from W_2 and gets replaced by the W_6, nearby water molecule (see also Fig. 6(b)). After the exchange, the proton embedding structure can now be pictured as a symmetrically solvated, Zundel-like cation, in which the two resonant partners, W_1 and W_2, act as HB donors exclusively to water molecules W_3, W_4, W_5, and the newly incorporated W_6 one. As such, this new solvation structure brings the donor-acceptor partners on an equal foot, benefiting the transfer process, which still requires an additional ~30 ps time interval to be fully accomplished.

Along the positive time branch, several recrossings take place during the next 50 ps following the proton stabilization in the W_2 molecule. In fact, the plots in the bottom panel reveal an opposite exchange process, between the W_4 water molecule (red line in Fig. 5(d)) and a nearby A_2 acetone (blue line in Fig. 5(d)), at $t \sim 55-70$ ps. Beyond this time, the original asymmetric solvation structure is recovered, "locking" temporarily the path to future transfers along the W_1-W_2 bond (see Fig. 6(c)).

As such, the previous description presents similarities and differences with the mechanisms controlling proton transfers in pure water.[45,48,49] For example, the aforementioned "locking" resembles the fourfold coordination of the pivot that would precede the last stage of successful proton transfer episodes in water (see, for example, Fig. 4 in Ref. 49). On the other hand, and as a clear distinctive feature, note that the key element that triggers the proton transfer in pure water is the absence of HB-acceptor character in the prospective new pivot,[45,48,49] whereas in A-W solutions, the key changes are operated in the HB-donor characteristics of this tagged molecule (which, incidentally, in $\mathcal{A}$-type solutions, remains always threefold coordinated). To support this line of reasoning, we further analyzed the concentration dependence of the composition of the second solvation shells, by building up histograms for the number of W molecules located in these regions. The results appear in Fig. 7: At $x_w \sim 0.8$, in ~80% of the configurations, already at least one out of the six molecules coordinated via HBs to the first solvation shell is A. We recall that this threshold concentration coincides with the location of the "kink" observed in the concentration dependences of k_{PT} (see Fig. 4) and in the – perhaps somewhat less evident – concentration dependence of the free energy barrier shown in the inset of Fig. 2. This feature would validate the hypothesis suggesting the onset of a new reactive mechanism regulating the interconversion kinetics that involves a W-A interchange as part of the second solvation shell of hydronium. By bringing the solvation structure of the donor and acceptor sites more symmetric (in terms of their HB donor characteristics), the scenario for the transfer would be energetically much more favorable than another one, in which the first solvation shell of an eventual, new pivot would include an A molecule.

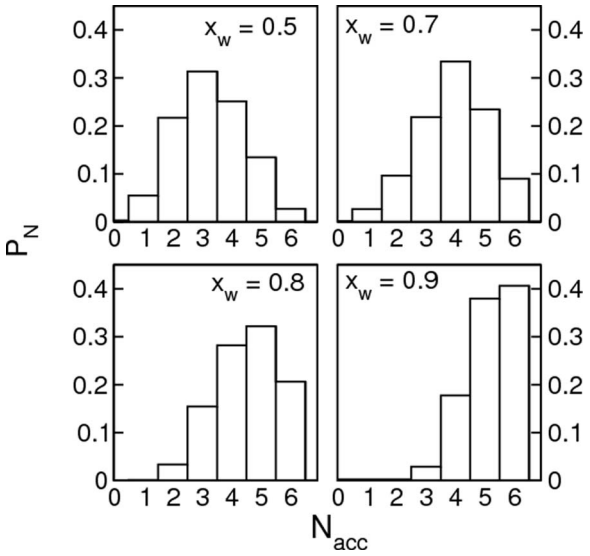

FIG. 7. Probability densities for the number of acceptor water molecules in the second solvation shell of H_3O^+, in different water-acetone solutions.

Before closing this section, we would like to briefly digress about our efforts to identify a relationship between proton-transfer rates and the persistence of long wavelength concentration fluctuations involving "clustered" water structures. To that end, we analyzed cumulative integrals of the type

$$N_{cl}(r) = 4\pi\rho_w \int_0^r r'^2\, h^{\dagger}_{o^*o_w}(r')\, dr', \tag{11}$$

where $h^{\dagger}_{o^*o_w}(r)$ represents the connectedness pair correlation function,[51] which is proportional to the conditional probability of finding a water molecule at a distance r, directly or indirectly connected to the pivot oxygen lying at the origin, via a continuous path of HBs. Results for $N_{cl}(r)$ for $\mathcal{A}$-type solutions with $x_w = 0.25$ and 0.5, are presented in the bottom panel of Fig. 1. For the sake of comparison, we have also included standard results for cumulative integrals of $g_{o^*o_w}(r)$. Two features are worth remarking: (i) For $x_w = 0.25$ solutions, the proton remains embedded within a "clustered" water domain comprising typically 10 water molecules. Moreover, the connectedness and the standard cumulative integrals detach from each other at $r \sim 7.5$ Å. This characteristic distance coincides with the location of the proton second solvation shell and reveals the presence of a sizable number of A molecules lying in this coordination shell, acting as "spacers." (ii) The scenario in $x_w = 0.5$ is qualitatively different, since the proton remains immersed within a fluctuating, tridimensional network of highly irregular shape, spanning across the complete length of the simulation box and involving approximately 80% of the W molecules in the sample. The presence of an already percolated structure at molar fractions as low as $x_w = 0.5$ (the actual percolative concentration threshold[52] was found to be $x_w^{perc} = 0.44$) and the absence of any relevant feature in the concentration dependence of our results

below this tagged concentration would suggest that the dynamics of proton transfers in $\mathcal{A}$-type solutions would not be controlled by the spatial characteristics of the prevailing hydrogen bonded structures with characteristic lengthscales that extend beyond ∼2−3 times the size of a water molecule.

C. Proton transport

The changes observed in the proton transfer kinetics will necessarily affect the mechanisms that govern the diffusion of protons in W-A mixtures. As such, one can reasonably anticipate that the decrease in the proton transfer rate will bring down the contributions of the Grotthuss mechanism to the resulting proton mobilities. A crude estimate of the extent of these contribution compared to the ones provided by the normal Stokes-like mechanisms can be rationalized in terms of simple geometrical arguments. Consider, for example, the case of $x_w = 0.25$ solutions: Our simulations show that it takes approximately $\tau \sim 40$ ps for the proton to make a $\ell_{tr} \sim 2.5$ Å, translocation jump. Moreover, during that time interval, considering a typical magnitude of the diffusion coefficient of W in these mixtures,[38] $D_w \sim 0.3$ Å^2 ps^{-1}, solvent molecules travel by ordinary hydrodynamic mechanisms a distance approximately four times longer, i.e., $\ell_{diff} \sim (6 D_w \tau)^{1/2} \sim 9$ Å. These numbers should be compared to those obtained for the case of pure water, where τ gets reduced by approximately one order of magnitude, bringing the distance traveled by the charge defect by ordinary diffusion comparable to the one describing translocations between neighboring water molecules.

A more precise quantitative analysis can be performed by analyzing diffusion coefficients D_{H^+} obtained from root mean square displacements of the excess charge in different mixtures, namely,

$$D_{H^+} = \frac{1}{6} \lim_{t\to\infty} \frac{\mathrm{d}\,\langle |\mathbf{r}_H(t) - \mathbf{r}_H(0)|^2 \rangle}{\mathrm{d}t}, \tag{12}$$

where the charge coordinate $\mathbf{r}_H(t)$ is defined in terms of a weighted sum of the coordinates of the EVB states participating in the EVB Hamiltonian,[11] namely,

$$\mathbf{r}_H(t) = \sum_{i=1}^{N_{EVB}} c_i^2\, \mathbf{r}_i^o(t). \tag{13}$$

Plots for the root mean square displacements appear in Fig. 8, whereas results for the concentration dependence of the proton diffusion coefficients in different W-A solutions are displayed in the inset. Note that the general trend of the latter values presents bimodal characteristics similar to the ones reported for k_{PT} and F^*: a sharp drop by a factor of ∼2, in passing from $D_{H^+} = 0.43$ Å^2 ps^{-1} for pure water down to $D_{H^+} = 0.2$ Å^2 ps^{-1} for $x_w = 0.8$ solutions, followed by a much milder descent along the $\mathcal{A}$-type realm, with $D_{H^+} = 0.15$ Å^2 ps^{-1} for the limiting $x_w = 0.25$ case.

For the sake of comparison, in the same inset, we have included two additional sets of results related to the previous one. The first one, depicted in open squares, corresponds to estimates of proton diffusion obtained from experimental results of limiting ionic conductivities Γ^0(MX) of MX electrolytes (MX = HCl and KCl) dissolved in W-A solutions,[53] namely,

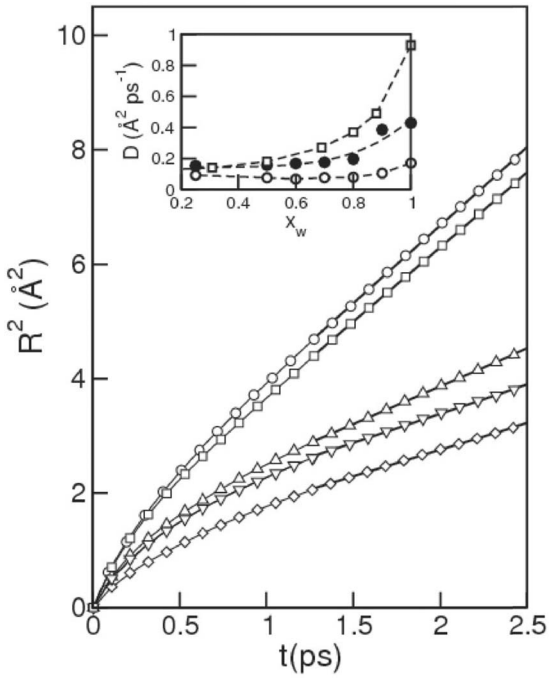

FIG. 8. Root mean square displacements for the proton coordinate in different W-A solutions: $x_w = 1$ (circles); $x_w = 0.9$ (squares); $x_w = 0.8$ (triangles up); $x_w = 0.7$ (triangles down); $x_w = 0.25$ (diamonds). The thick solid lines correspond to linear fits for $t > 1.25$ ps. The inset includes results for the diffusion coefficients for H^+ (black circles), experimental results taken from Ref. 53 (open squares) and Li^+ (open circles).

$$D_{H^+} \sim \frac{\Gamma^0(\mathrm{HCl}) - 0.5\,\Gamma^0(\mathrm{KCl})}{k_B T N_A e^2}. \tag{14}$$

In the previous expression, k_B is Boltzmann constant, whereas N_A and e represent the Avogadro number and the electron charge, respectively. One can see that the major discrepancies between experimental and simulated results for the diffusion coefficients are found in $\mathcal{B}$-type solutions, where the latter values are a factor of ∼2 smaller than the former ones. This is a well documented deficiency of EVB Hamiltonians,[11–13] whose origins have been discussed in previous studies.[10,54] Interestingly, however, these discrepancies tend to diminish as we move towards $\mathcal{A}$-type solutions where, for example, the difference falls down to only 15%, for $x_w \sim 0.25$. The second set of results (shown in open circles) corresponds to simulation results for the diffusion coefficients for an infinite diluted, small size cation, such as Li^+. Parameters for interactions involving this cation were taken from Ref. 55. One can clearly see that the proton diffusion differs by a factor of ∼2 in $\mathcal{B}$-type solutions, where contributions to the Grotthuss mechanism to the diffusion still prevail whereas, in $\mathcal{A}$-type solutions, the magnitudes of the diffusion coefficients of the two species become gradually much more comparable. This feature may bring additional support to the hypothesis that the differences in the diffusion coefficients in W-rich solutions might be traced back to an underestimation of the proton transfer rate.[11,12]

IV. CONCLUDING REMARKS

In this paper, we have presented a microscopic description of equilibrium and dynamical characteristics pertaining to the solvation of protons in solutions combining water and acetone. In particular, we found that, for solutions with water content down to $x_w \sim 0.25$, the incorporation of the aprotic component does not modify the coordination of the excess charge at short distances in a sensible fashion. As such, the proton first solvation shell still involves three tightly bound water molecules, with no relevant HOH...$[O^*H_3]^+$ acceptor connectivity. We did find modifications in the relative stabilization of Eigen vs Zundel structures. In this respect, as we move to A-rich solutions, Zundel configurations become gradually less infrequent, a fact that would reveal a weakening of the HB joining resonant partners and eventual modifications of the strength of polarization fluctuations with the incorporation of the aprotic component.

From the dynamical side, the destabilization of Zundel-like structures necessarily affects the dynamics of proton transfer. In passing from the pure water case down to $x_w \sim 0.8$ solutions, proton transfer rates present a sharp drop, followed by a somewhat milder concentration dependence for the rest of A-rich solutions investigated. As a result, the characteristic temporal scale describing translocation episodes stretches by approximately one order of magnitude, as one compares the pure water case and the $x_w = 0.25$ one.

Looking for clues to rationalize the origins of such variations, we monitored several relevant geometrical parameters describing the solvation structures along many translocations in A-rich solutions. Similar to what has been reported in the pure water case, our results showed that successful transfer episodes are triggered by modifications operated in the second solvation shell of the excess charge. However, here, the modifications do not involve a HB cleavage but an exchange between an A molecule and a nearby W one. This alteration leads to Zundel-like structures in which each one of the donor/acceptor partners is solvated by two, HB acceptor water molecules in an equivalent fashion. As such, this scenario opens the possibility of transfers, in which the first solvation shells of the prospective proton acceptor sites are composed exclusively by three water molecules. The analysis of the compositions of the proton second solvation shells reveals that A molecules start to participate in the proton second solvation shell in a meaningful percentage of configurations, in solutions with concentrations close to the threshold value $x_w^{thr} \sim 0.8$. Consequently, below x_w^{thr} transfers should gradually become also dependent on a new timescale describing the interchange of A and W as part of the proton second solvation shell, which should necessarily stretch, as we move to A-richer solutions.

The modifications operated in the translocation dynamics necessarily affect the relative contributions from the Grotthuss classical translocation mechanism to the overall proton diffusion. The concentration dependence of the diffusion coefficient shows similar signs of a bimodal character: (i) a drop by a factor of $\sim$2 in passing from the pure water case down to x_w^{thr}, followed by (ii) practically a plateau-like behavior as we move to A-richer solutions. Interestingly, in the latter region the agreement between simulation predictions and direct experimental results seems to improve, compared to the pure water case. Moreover, in this concentration regime, and as a consequence of the gradual deactivation of the translocation mechanism, proton diffusion becomes much more comparable to the one exhibited by a small-size ion, such as Li^+. Finally, we also remark that the analysis of the evolution of HB-clustered structures around the excess charges did not provide any clear evidence of eventual relationships between the concentration dependences of proton rates and/or diffusion constants, and the onset of percolative-like phenomena.

ACKNOWLEDGMENTS

D.L. is a staff member of CONICET-Argentina.

[1] M. Eigen and L. de Maeyer, Proc. R. Soc. London Ser. A **247**, 505 (1958).
[2] G. Zundel and H. Metzger, Z. Phys. Chem. **58**, 225 (1968).
[3] R. Vuilleumier and D. Borgis, J. Phys. Chem. B **201**, 4261 (1998).
[4] R. Vuilleumier and D. Borgis, Chem. Phys. Lett. **284**, 71 (1998).
[5] R. Vuilleumier and D. Borgis, in *Classical and Quantum Dynamics in Condensed Phase Simulations*, edited by B. J. Berne, G. Ciccotti, and D. F. Coker (World Scientific, Singapore, 1998), Chap. 30.
[6] M. Tuckerman, K. Laasonen, M. Sprik, and M. Parrinello, J. Chem. Phys. **103**, 150 (1995).
[7] M. Tuckerman, K. Laasonen, M. Sprik, and M. Parrinello, J. Phys. Chem. **99**, 5794 (1995).
[8] D. Marx, M. E. Tuckerman, and M. Parrinello, J. Phys.: Condens. Matter **12**, A153 (2000).
[9] D. Marx, M. E. Tuckerman, J. Hutter, and M. Parrinello, Nature (London) **397**, 601 (1999).
[10] U. W. Schmitt and G. A. Voth, J. Chem. Phys. **111**, 9361 (1999).
[11] T. J. F. Day, A. V. Soudackov, M. Cuma, U. W. Schmitt, and G. A. Voth, J. Chem. Phys. **117**, 5839 (2002).
[12] Y. Wu, H. Chen, F. Wang, F. Paesani, and G. A. Voth, J. Phys. Chem. B **112**, 467 (2008).
[13] K. Park, W. Lin, and F. Paesani, J. Phys. Chem. B **116**, 343 (2012).
[14] S. Walbran and A. A. Kornyshev, J. Chem. Phys. **114**, 10039 (2001).
[15] A. A. Kornyshev, A. M. Kuznetsov, E. Spohr, and J. Ulstrup, J. Phys. Chem. B **107**, 3351 (2003).
[16] A. Luzar and D. Chandler, Nature (London) **379**, 55 (1996).
[17] A. Luzar and D. Chandler, Phys. Rev. Lett. **76**, 928 (1996).
[18] C. J. T. Grotthuss, Ann. Chim. **LVIII**, 54 (1806).
[19] Z. Stein and E. Gileadi, J. Electrochem. Soc. **132**, 2166 (1985).
[20] E. Gileadi and E. Kirowa-Eisner, Electrochim. Acta **51**, 6003 (2006).
[21] M. K. Petersen and G. A. Voth, J. Phys. Chem. B **110**, 7085 (2006).
[22] J. A. Morrone, K. E. Haslinger, and M. E. Tuckerman, J. Phys. Chem. B **110**, 3712 (2006).
[23] A. Warshel and R. M. Weiss, J. Am. Chem. Soc. **102**, 6218 (1980).
[24] A. Warshel, *Computer Modelling of Chemical Reactions in Enzymes and Solutions* (Wiley, New York, 1991).
[25] J. Aqvist and A. Warshel, Chem. Rev. **93**, 2523 (1993).
[26] J. M. J. Swanson, C. M. Maupin, H. Chen, M. K. Petersen, J. Xu, Y. Wu, and G. A. Voth, J. Chem. Phys. B **111**, 4300 (2007).
[27] M. K. Petersen, S. S. Iyengar, T. J. F. Day, and G. A. Voth, J. Phys. Chem. B **108**, 14804 (2004).
[28] S. Iuchi, H. Chen, F. Paesani, and G. A. Voth, J. Phys. Chem. B **113**, 4017 (2009).
[29] S. Feng and G. A. Voth, J. Phys. Chem. B **115**, 5903 (2011).
[30] Z. Cao, Y. Peng, T. Yan, S. Li, A. Li, and G. A. Voth, J. Am. Chem. Soc. **132**, 11395 (2010).
[31] C. Dellago, M. M. Naor, and G. Hummer, Phys. Rev. Lett. **90**, 105902 (2003).
[32] J. Xu, S. Izvekov, and G. A. Voth, J. Phys. Chem. B **114**, 9555 (2010).
[33] J. Rodriguez, J. Marti, E. Guàrdia, and D. Laria, J. Phys. Chem. B **111**, 4432 (2007).
[34] D. Laria, J. Martí, and E. Guàrdia, J. Am. Chem. Soc. **126**, 2125 (2004).
[35] A. Estrada-Baltazar, A. De Leon-Rodriguez, K. R. Hall, M. Ramos-Estrada, and G. A. Iglesias-Silva, J. Chem. Eng. Data **48**, 1425 (2003).

[36]A. Streitwieser, Jr. and C. H. Heathcock, *Introduction to Organic Chemistry* (MacMillan, London, 1985).
[37]R. P. Feynman, Phys. Rev. **56**, 340 (1939).
[38]A. Perera and F. Sokolić, J. Chem. Phys. **121**, 11272 (2004).
[39]S. Weerasinghe and P. E. Smith, J. Chem. Phys. **118**, 10663 (2003).
[40]J. C. Berendsen, J. P. M. Postma, W. F. Von Gusteren, and J. Hermans, in *Intermolecular Forces*, edited by B. Pullman (Reidel, Dortrecht, 1981).
[41]P. Jedlovszky, A. Idrissi, and G. Jancs, J. Chem. Phys. **130**, 124516 (2009).
[42]M. Kang, A. Perera, and P. E. Smith, J. Chem. Phys. **131**, 157101 (2009).
[43]P. Jedlovszky A. Idrissi, and G. Jancs, J. Chem. Phys. **131**, 157102 (2009).
[44]L. X. Dang and B. M. Pettitt, J. Phys. Chem. **91**, 3349 (1987).
[45]O. Markovitch, H. Chen, S. Izvekov, F. Paesani, G. A. Voth, and N. Agmon, J. Phys. Chem. B **112**, 9456 (2008).
[46]C. Knight and G. A. Voth, Acc. Chem. Res. **45**, 101 (2012).
[47]A. Chandra, M. E. Tuckerman, and D. Marx, Phys. Rev. Lett. **99**, 145901 (2007).
[48]N. Agmon, Chem. Phys. Lett. **244**, 456 (1995).
[49]T. C. Berkelbach, H.-S. Lee, and M. E. Tuckerman, Phys. Rev. Lett. **103**, 238302 (2009).
[50]T. J. F. Day, U. W. Schmitt, and G. A. Voth, J. Am. Chem. Soc. **122**, 12027 (2000).
[51]T. DeSimoni, S. Demoulini, and R. M. Stratt, J. Chem. Phys. **85**, 391 (1986).
[52]N. A. Seaton and E. D. Glandt, J. Chem. Phys. **86**, 4668 (1987).
[53]T. K. Brownson and F. M. Cray, J. Chem. Soc., Trans. **127**, 2923 (1925).
[54]U. W. Schmitt and G. A. Voth, Chem. Phys. Lett. **329**, 36 (2000).
[55]I. S. Joung and T. E. Cheatham III, J. Phys. Chem. B **112**, 9020 (2008).